Data-fusion of high resolution X-ray CT, SEM and EDS for 3D and pseudo-3D chemical and structural characterization of sandstone.

Wesley De Boever*[1], Hannelore Derluyn[1], Denis Van Loo[2], Luc Van Hoorebeke[3], Veerle Cnudde[1]

1. PProGRess – UGCT / Department of Geology and Soil Science / Ghent University, Ghent – Belgium / Wesley.deboever@ugent.be

2. X-ray Engineering bvba – www.XRE.be - Ghent, Belgium

3. UGCT – Department of Physics and Astronomy / Ghent University, Ghent - Belgium

*corresponding author: Wesley De Boever – Krijgslaan 281 – 9000 Ghent – Belgium

e-mail: Wesley.deboever@ugent.be / tel: +32(0)9 264 4633

Abstract

When dealing with the characterization of the structure and composition of natural stones, problems of representativeness and choice of analysis technique almost always occur. Since feature-sizes are typically spread over the nanometer to centimeter range, there is never one single technique that allows a rapid and complete characterization. Over the last few decades, high resolution X-ray CT (µ-CT) has become an invaluable tool for the 3D characterization of many materials, including natural stones. This technique has many important advantages, but there are also some limitations, including a tradeoff between resolution and sample size and a lack of chemical information. For geologists, this chemical information is of importance for the determination of minerals inside samples. We suggest a workflow for the complete chemical and structural characterization of a representative volume of a heterogeneous geological material. This

workflow consists of combining information derived from CT scans at different spatial resolutions with information from scanning electron microscopy and energy-dispersive X-ray spectroscopy.

Keywords: X-ray tomography; μ-CT; scanning electron microscopy; energy-dispersive spectroscopy; data fusion

1. Introduction

Investigation of natural stones, and the behavior of fluids in their pore networks, is important in many scientific fields. This includes the study of reservoir rocks, which is important for the oil and gas industry (Antrett, 2013; Jiao et al., 2014), but also for hydrogeology and water management studies (Cirpka et al., 2014; Lagrou et al., 2004). Pore-scale processes, such as ice (De Kock et al., 2013; Matsuoka and Murton, 2008) or salt precipitation (Derluyn et al., 2013) and carbonatation, also have a big influence on the weathering of building stones (Dewanckele et al., 2014), the behavior of pavement materials, or the cracking of concrete. A full characterization of the complex microstructure of porous media is thus of vital importance to understand and predict the processes regulating the phenomena mentioned above. For many of the materials that are common in these research fields, one main difficulty to overcome is the multi-scale character of their structure. Geological materials are composed of a mixture of macro- to micro- and even nano-scale features. Furthermore, their composition is very heterogeneous and can vary drastically over a distance of just centimeters. These inhomogeneous characteristics make it very difficult to find and combine techniques that can analyze samples over different length scales, since it is often of interest to analyze centimeter-scale samples at nanometer-precision.

Another layer of complexity in the understanding of pore-scale processes in natural stones is that these processes are not only influenced by the pore structure, but also by the chemical composition of the material. In this work, a combination of different techniques is proposed, using a well-defined workflow, to acquire as much information as possible on the structure and composition of a sandstone sample. This work focuses on high resolution X-ray CT (µ-CT) and scanning electron microscopy (SEM) combined with energy dispersive X-ray spectroscopy (EDS) (Reed, 2005) and focused ion beam nanotomography (FIB-nt) (Holzer et al., 2004; Keller et al., 2011).

Over the last few decades, µ-CT has become an invaluable tool for the 3D characterization of many materials, including natural stones (Cnudde and Boone, 2013; Ketcham and Carlson, 2001; Wildenschild and Sheppard, 2013). Although there are many important advantages for this technique, there are also some limitations. A first shortfall of µ-CT is that high-resolution analysis always requires small samples, even in µ-CT systems using magnification optics; although nanofocus X-ray tubes can have a focal spot size down to about 400 nm, this spatial resolution can only be achieved by imaging extremely small (less than 1 mm) samples (Al-Raoush and Papadopoulos, 2010). This leads to questions about representative elementary volume (REV), particularly for heterogeneous geological samples. Second, the lack of chemical information in µ-CT datasets is a big shortcoming for geologists, as this chemical information is of importance for the determination of minerals present in samples. Although a rough estimate or relative relationship between the densities and atomic number of the elements in the sample can be determined, quantitative values remain a challenge (Jussiani and Appoloni, 2014). This mineralogical information is of importance for the understanding of various processes that happen in the pore space of geological materials, including migration of (saline or acid) fluids (Derluyn et al., 2013) and

dissolution and precipitation reactions (Dewanckele et al., 2012). In an effort to try to enhance the information acquired by µ-CT, additional experiments using different methods can be executed. More exactly, we propose a workflow combining µ-CT with 2D imaging techniques (SEM and EDS), and using image registration for a one-to-one fusion of the data. Data fusion of CT and 2D microscopy techniques was already done by Huddlestone-Holmes and Ketcham (2005), proving the complementarity of both methods. Over the past decade, image quality and registration techniques have improved, and 3D registration algorithms have become accessible to researchers.

SEM can provide 2D images of large surfaces, at much higher resolutions than µ-CT (less than 10 nm for secondary electron images; Reed, 2005). Since images can be tiled into a mosaic image, there is no real limit to the surface that can be analyzed. Combining µ-CT with SEM images can improve information on microporosity and microstructure of analyzed samples (Sok et al., 2010). When combined with EDS, the chemical composition can be analyzed as well, to allow the visualization of spatial distribution of different mineral phases.

2. Materials and methods

2.1. The Vosges sandstone

For this research, a material had to be used that was heterogeneous in terms of structure and mineralogy. Simple sandstones (e.g. Bentheimer sandstone; Nijland et al., 2004) are not suited because they require far less analysis to understand their structure. For this methodological study, a stone was required with a structure possessing a good variation between macropores (> 20 µm) and micropores (< 1 µm), and a significant amount of clays and feldspars to ensure enough chemical variation.

Therefore, a variety of Vosges sandstone, the *grès a Meule,* was selected. This fine-grained pink sandstone from the east of France consists of about 65 % quartz, around 25 % feldspars and about 10 % clay minerals such as micas, smectites and kaolinite (Schmitt et al., 1994); its average porosity is around 22 % (Bésuelle et al., 2000). The stone is found in the lower part of the *grès à Voltzia* formation, a local term for a part of the Buntsandstein formation, deposited in the lower Triassic (Gall and Grauvogel-Stamm, 2005; Shear et al., 2009) and has been mainly used as a local building stone and milling stone.

2.2. Methods

A workflow was developed to combine information from µ-CT, SEM, EDS and FIB-nt. The base sample of the entire study was a 14 mm, cuboid Vosges sandstone sample (Figure 1). This sample was embedded in resin to ensure mechanical strength, and polished down to 1/4 µm accuracy. The first step was a 'medium resolution' CT scan of the entire sample, at the best spatial resolution (9 µm) possible for that sample size (Figure 1, 1), using the HECTOR setup (Masschaele et al., 2013a) of the Ghent University Centre for X-ray Tomography (UGCT, www.ugct.ugent.be). Next, SEM images and EDS mappings for three of the main occurring elements (silicon, potassium and iron; determined by point measurements of the ray spectrum) were performed on all 5 exposed surfaces of the sample (Figure 1, 2). Thereafter, a small, 1 mm diameter cylindrical subsample was drilled out of the main sample, and scanned at high resolution (0.86 µm) using UGCT's MEDUSA setup (Figure 1, 3). We leave the option open to perform other, higher-resolution techniques on this small micro-plug (at resolutions <100 nm), to study regions of the sample in 3D which were too fine-grained for µ-CT (Figure 1, 4).

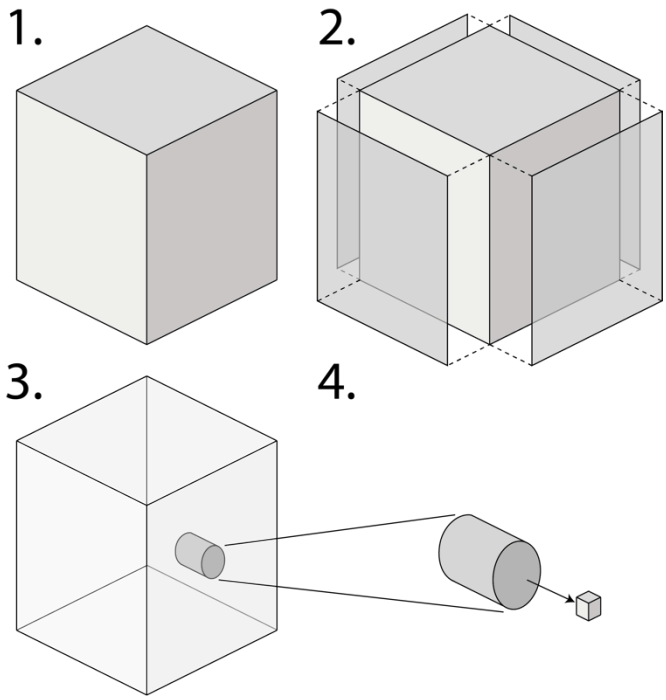

Figure 1: Schematic representation of the workflow for this study. 1) 14 mm sample for medium resolution CT. 2) SEM and EDS mappings of the 5 exposed sides of the sample. 3) Extraction of 1 mm diameter sub-sample for high-resolution CT. 4) Possibility of further investigation of sub-sample using other, high-resolution techniques.

2.2.1. X-ray computed tomography

Image acquisition

µ-CT scans were performed at the UGCT. Two different setups were used, one for the medium resolution, and another one for the high resolution scans. For the medium resolution scans, HECTOR (High Energy CT Optimized for Research; (Masschaele et al., 2013b)) was used. This system uses a microfocus directional target X-ray source up to 240 kV and 280 W (XWT 240-SE, from X-RAY WorX) and a large flat-panel detector (40 x 40 cm^2 PerkinElmer 1620 CN3 CS). For this experiment, the source was operated at a voltage of 150 kV and a power of 10 W. 2000 projections were taken at an exposure time of 2 s. The voxel size of this dataset was 8.9 µm.

High-resolution CT scans were performed on the new MEDUSA setup of the UGCT, which is equipped with a Varian PaxScan 2520 a-Si flat-panel detector. A transmission type X-ray tube (X-RAY WorX THC) was used for this experiment. 2800 projections were taken,

with an exposure time of 1.5 s. The tube voltage for this experiment was 90 kV. Using these parameters, a spatial resolution of 0.86 μm was reached. Both systems were developed in-house at the UGCT, in collaboration with the spin-off company X-Ray Engineering bvba (www.XRE.be).

Reconstruction and Image Analysis

For the reconstruction of the raw projections, the in-house developed Octopus reconstruction software was used (Vlassenbroeck et al., 2007) (www.octupusreconstruction.eu). Image analysis was done using UGCT's Morpho+ software (Brabant et al., 2011), which has recently been commercialized by InsideMatters (www.octopusanalysis.eu), and with Avizo® (www.vsg3d.com).

2.2.2. Scanning electron microscopy and Energy Dispersive X-ray spectroscopy

For each of the exposed surfaces of the sample (top surface and 4 lateral surfaces), a grid of SEM images was acquired to compose a photomosaic of the entire surface. The analysis was performed on a JEOL 5310-LV system, equipped with a secondary and backscattered electron detector and an Oxford Instruments silicon-drift detector for EDS analysis. A total of 300 backscattered SEM images were acquired at each plane, resulting in a total of 1500 images, which had to be taken manually since the JEOL 5310 is not equipped with automated stage control. The SEM was operated at 20 kV with a spot size of 13 nm and a working distance of 20 mm. Images were stitched together using the Microsoft Image Composite Editor (ICE; http://research.microsoft.com), which has algorithms for automatic grid-based registration of images. Next, EDS mappings were obtained, at 24 to 28 images per side. Due to time restrictions, only half of the surface of the SEM photomosaics was covered, at half the magnification. This resulted in 125 separate acquisitions, taking over 40 hours to acquire the data.

2.2.3. Data fusion

Image registration was used to link the information from the different techniques. For various reasons it was very difficult to do this registration using automated algorithms: images were acquired using different techniques and different detectors, meaning that the form of corresponding features in images captured with different methods was not completely the same. This effect occurs since the angles of the 14 mm sample were not completely straight, and SEM imaging was therefore not always performed with a beam perpendicular to the sample surface. Furthermore, the direction of the CT slices in the vertical plains was never completely parallel or perpendicular to the samples surfaces. Furthermore, SEM images provide a depth of view beyond the sample surface, which is absent in 2D CT slices. This is usually an advantage of SEM imaging, but proves to be a disadvantage for registration. To overcome these issues, landmark-based registration was employed. Corresponding points in the reference and transformed image were manually selected. The transformation to match those two point groups was then calculated and images were transformed or warped using the same transformation equation. If there was only rigid-body movement, and no deformation, a simple rigid transformation algorithm could be used to register the two images. However, due to the use of different detectors and techniques, distortion was present in the images, and an algorithm called Bookstein Image Warp (Bookstein, 1989) was used to register the images. Using this algorithm, points from the transformed group were forced to fit the reference points, and all image points in between were shifted by using correlation of the surrounding points (Bookstein, 1989). In this research, three types of registration were necessary: 2D to 2D registration to match EDS data to the SEM images, 2D to 3D registration to match these data to the 3D CT volume, and 3D to 3D registration to identify the location of the sub-sample in the base sample. In the first case, only X/Y

transformation was necessary, whereas in the other cases, rotation and translation in three dimensions had to be performed.

3. Results

3.1. X-ray computed tomography

The first CT scan at medium resolution (voxel size: 8.9 μm) provides a good insight regarding the distribution of dense inclusions (mostly titanium oxides), and gives an idea about the internal structure of the stone. Most of the rest of the solid matrix had about the same grey value, so there is hardly any contrast between the quartz grains and other mineral phases present (Figure 2, left). Further, the size of the grains and of the pore system makes it impossible to perform a decent analysis of grain/pore shape and size. Image analysis with Morpho+ (Brabant et al., 2011) resulted in a porosity of 9.04 %, consisting of 5.4 % open porosity (connected to the outside of the sample) and 3.6 % closed porosity. This high amount of closed porosity is not normal for a sandstone like the Vosges sandstone (Bésuelle et al., 2000), and can only be explained by the lack of spatial resolution in the dataset. Attention has to be drawn to the high dependency of results on choices made during image segmentation. A small difference in threshold value causes high changes in resulting porosity, meaning that the resolution of this CT scan is just not high enough for decent analysis of the sample. High resolution scanning of the 1 mm microplug (voxel size: 0.86 μm) resulted in a much better scan where porosity was clearly resolved; boundaries between porosity and grains were very sharp (Figure 2, right), meaning that results from image segmentation can be considered reliable. Grains and pores could be segmented, and the total porosity by image analysis was found to be 16.50 %, of which only 0.2 % was characterized as closed porosity. In

the high-resolution images, there was contrast between quartz grains, feldspars and clay minerals, and dense minerals. However, contrast between quartz and feldspars and clays was not enough to analyze each individual phase.

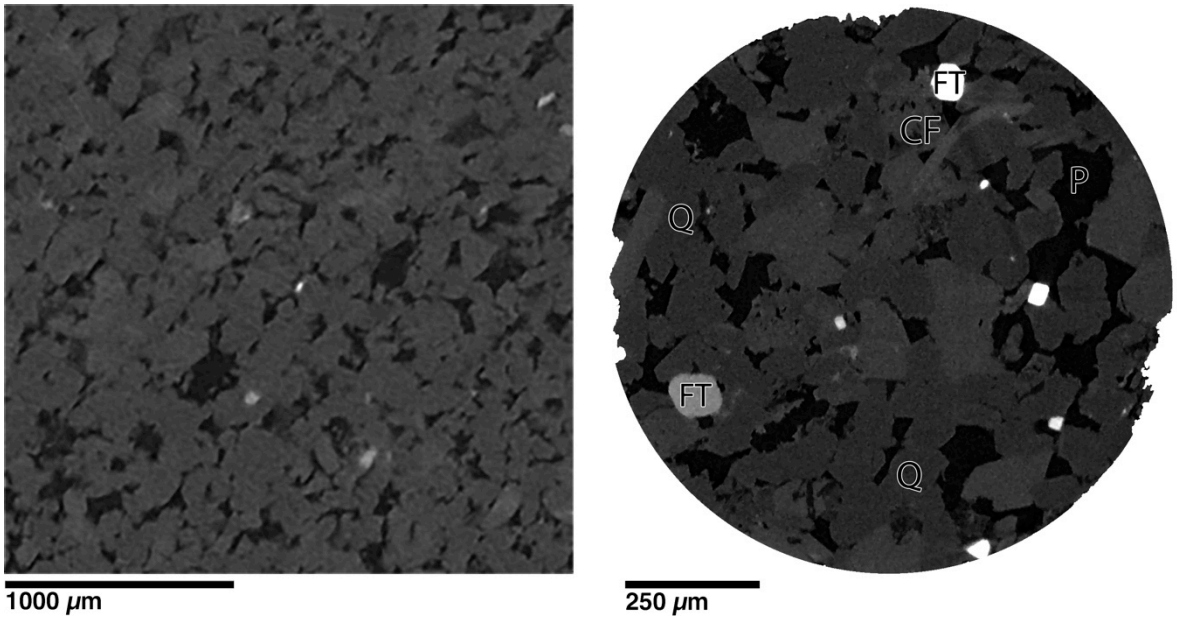

Figure 2: Left: detail of 2D slice from medium resolution CT scan (voxel size: 9 μm); right: 2D slice from high resolution CT scan (voxel size: 0.86 μm). Image quality is much better in the high-resolution scan, so sample analysis is much more accurate than for the low resolution scan. Annotations: Q = quartz, CF = clays and feldspars, FT = iron and titanium oxides, P = pore.

3.2. Scanning electron microscopy and Energy Dispersive X-ray spectroscopy

As a result of the SEM analysis, panoramic images of each surface of the sample were obtained. At the magnification that was used, the pixel size in the images was 1.08 μm. This is about one order of magnitude better than the resolution of the medium CT scan, i.e. compared to the 8.9 μm voxel size of the CT scan of the entire sample. Contrast in the BSE images is visible between quartz and feldspars, albeit not very clear at the energy and spot size used. The dense titanium oxides show a very high contrast with respect to the other minerals, but are rather scarce in the 2D planes. EDS mappings revealed the distribution for silicon, potassium and iron. Grains which are very rich in silicon can be determined as quartz (SiO_2) grains, zones rich in potassium are feldspars ($KAlSi_3O_8$) or clay minerals (e.g. muscovite: $KAl_2(AlSi_3O_{10})(F,OH)_2$) and iron-rich zones are areas

where iron oxides are present. The images indicate a rather uniform distribution of quartz, feldspars and clay minerals throughout the entire sample; however, the iron is mainly present in a distinct layer, mainly on two of the five surfaces. It is also apparent that most of the iron is not present in the form of grains, but is often located inside the cement that binds these grains together (Figure 3).

These results prove that SEM combined with EDS gives a good idea about the presence of different mineral phases inside the investigated sample, and that EDS is still a useful tool that can reveal the presence of different mineral phases, even if there is no compositional variance visible in SEM images. Furthermore, distribution of these phases in the 2D surfaces of the material is easily observed and analyzed.

3.3. Image registration

2D-to-2D

2D-to-2D image registration between SEM and EDS images provides grain-to-grain information about mineralogy, even when contrast in BSE images is too low (Figure 3). Image registration was done using landmarks, which are very easy to detect, since both images have almost the same feature shape and the orientation of the images is the same. Due to the depth of view in SEM images (images show information beyond the absolute surface of the sample) it is very difficult to use automated algorithms. We remark that this step is not necessary on most modern SEM machines, as they can link SEM and EDS data automatically however it is necessary if the SEM machine is not equipped with an automated stage control, as was the case in this research. This method allows combination of SEM images with chemical information derived from other techniques as well, such as micro-X-ray fluorescence (μ-XRF) (Boone et al., 2011).

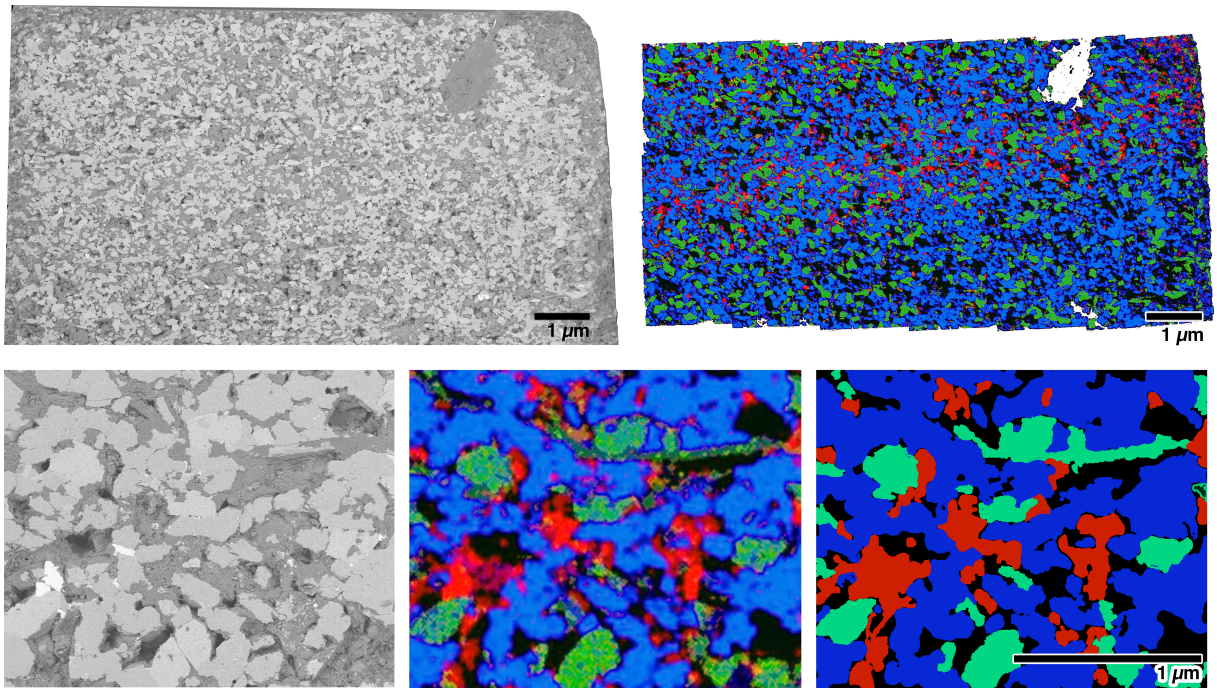

Figure 3: Top: SEM image and corresponding EDS map. Blue = Quartz, Green = Clays and Feldspars, Red = Iron oxides.
Bottom: Left: detail of SEM image; middle: detail of EDS map; right: simplified representation of EDS map. Grains can be identified individually as different minerals.

2D-to-3D

Although both CT and SEM/EDS images reveal a lot of information on the structure and mineralogy of the sample, this information becomes much more useful if the orientation and distribution of the different mineral phases can be linked directly to the 'low-resolution' CT volume. This way, 3D orientation of certain layers can be observed and measured. After registration of the 2D SEM and EDS images to the 3D volume, we can see the orientation of the iron-rich layer that was described in the previous paragraph (Figure 3 and Figure 7). Although the SEM and EDS images are in 2D, this method yields a pseudo-3D look at the distribution of the iron inside the sample.

2D to 3D image registration of SEM (and EDS) images to the CT volume is not straightforward, and besides the depth of view difference, corresponding features in both image sets do not have the exact same form. This effect occurs since the angles of the 14 mm sample were not completely straight, and SEM imaging was therefore not

always performed with a beam perpendicular to the sample surface. Furthermore, the direction of the CT slices in the vertical plains was never completely parallel or perpendicular to the samples surfaces Figure 4 shows that corresponding features can be recognized, but shapes and sizes in both images are not completely the same. Additionally, the visual information beyond the sample surface makes it difficult to directly link the SEM images to CT slices, as grain boundaries are far more difficult to detect in the SEM images. Landmarks were selected manually after visually looking for corresponding zones in the CT volume and SEM images (Figure 4). Landmarks in the CT volume were spread across 50 to 100 slices, since sample surfaces were not perfectly parallel to the orientation of the slices. Since manual placement of landmarks creates an inevitable error, about 100 locations per surface were selected as registration landmark, to average out this error. This proved to be enough for a qualitative grain-to-grain match between different datasets. Registration was done in two steps: first a rigid rotation was performed to rotate the SEM images in the same planes of the surfaces of the volume, using only four landmarks in the corners of both the SEM image and the corresponding surface in the SEM volume. Afterwards, an X/Y translation step was performed, combined with image warping to compensate for the difference in feature form in both imaging methods.

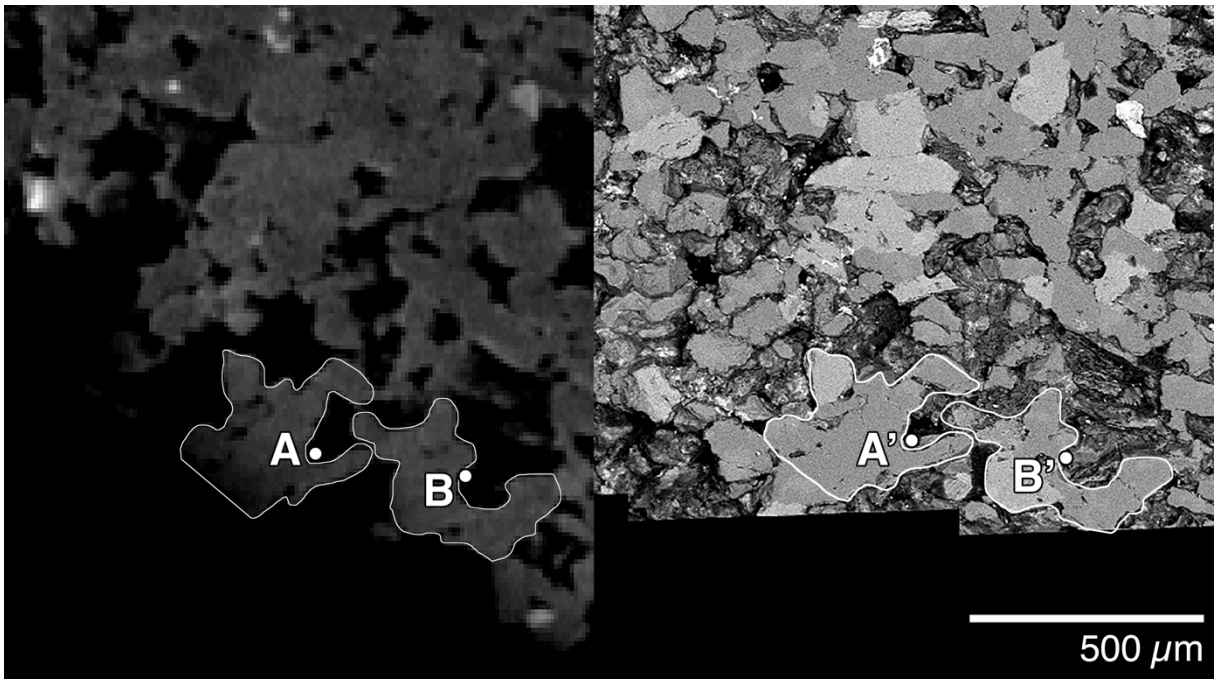

Figure 4: 2D to 3D image registration. White lines indicate corresponding areas in CT slice (left) and SEM image (right). White dots indicate possible points for landmark placement (A, A' and B, B').

3D-to-3D

The final type of image registration links the reconstructed microplug CT scan to the larger CT scan of the base sample (3D-to-3D registration). Since geological materials like the Vosges sandstone and other construction materials such as concrete and bricks, are heterogeneous in nature, it is important to pinpoint the location of a sub-sample. If a sub-sample is very small (in this case, < 1 mm), the properties derived from this one microplug might not be representative for the entire sample. As in the 2D-to-3D registration step, semi-automatic landmark registration was performed to create the alignment between the small and large 3D volume and this time, rigid transformation was used to align the images. It should be stressed that the resolution in the lowest resolution CT scan was insufficient for direct selection of these landmarks. Even more, the 2D-to-3D registration of the SEM images to the low-resolution scan is an absolute must if one wants to know the exact location of the microplug in the large sample. Figure 5 shows that first, landmarks A and B were selected in the low-resolution tomogram and

the SEM image. Finding landmark A in the high-resolution scan was much more easy, as spatial resolution and contrast are high enough in that volume. A combination of these points, together with some other points, made it possible to register the microplug into the cuboid.

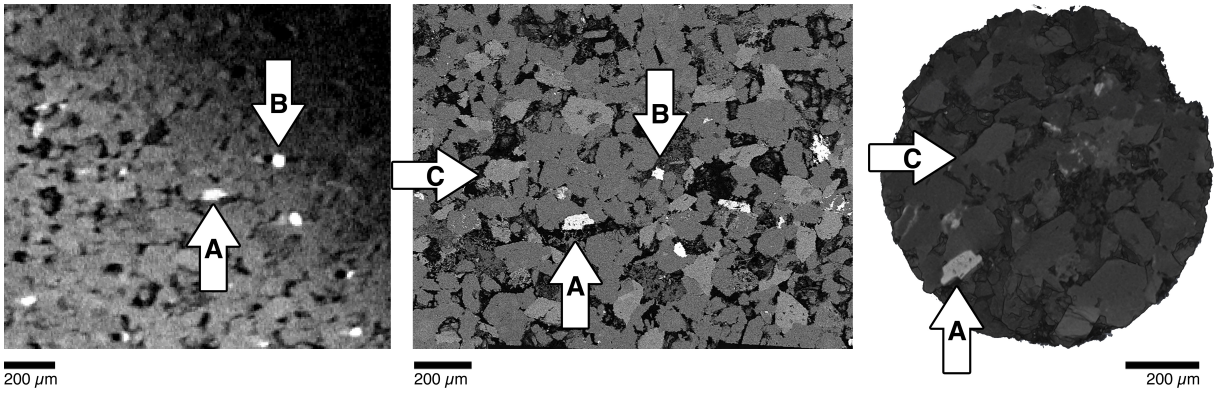

Figure 5: 3D-to-3D registration using landmarks. Left: Low-resolution CT; center: Registered SEM image; Right: High-resolution CT. The SEM image in the middle is used as an intermediary image to be able to find corresponding points.

Figure 6 shows the importance of this last image registration step. The small microplug is indicated in red inside the larger sample, which has been partially made transparent. High-density minerals are not distributed uniformly throughout the sample, and porosity is not the same throughout the entire sample. Indication of the location of the first subsample can help to set a strategy for further subsampling, or to determine which zones in the sample will have the same (flow) parameters as the microplug.

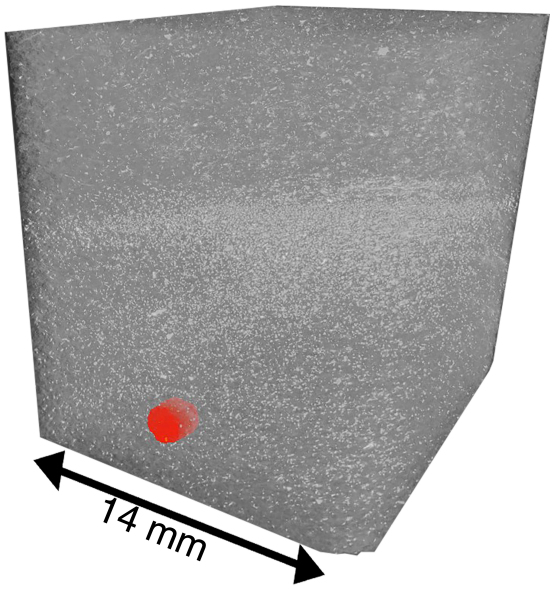

Figure 6: Location of the microplug (Ø = 1 mm) in the full sample (width = 14 mm). The partially transparent full sample reveals that dense minerals, i.e. represented in lighter grey, are unevenly distributed throughout the material.

4. Discussion

Location and orientation of different mineral zones inside a sample

SEM combined with EDS gives useful information about the presence of different mineral phases inside the investigated sample. Furthermore, the distribution of these phases in the 2D surfaces of the material is easily observed and analyzed. When 2D mineral distribution maps are registered to the surfaces of a 3D volume, a pseudo-3D-look at the orientation and distribution of these minerals is obtained. This means that the iron-rich laminations can not only be observed, but also spatially oriented in the sample (Figure 7, 3). This orientation can be compared to that of other features in the sample, and extrapolated to the sample's interior.

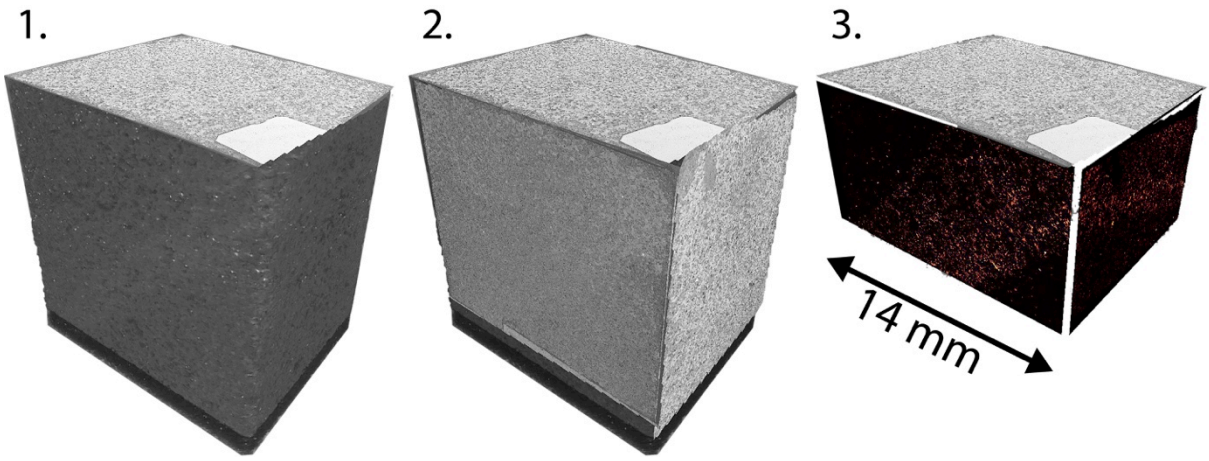

Figure 7: 1) Medium resolution CT volume with 1 SEM image registered to the top surface. 2) All SEM images registered to the surfaces of the CT volume. 3) EDS map for iron registered to two sides of the sample, showing the orientation of the observed iron oxide laminations.

Location of the sub-sample inside the base sample

Since geological materials like the Vosges sandstone are heterogeneous in nature, it is important to pinpoint the location of sub-samples in their parent sample. Zones with different structures or composition cannot always be identified in a macroscopic way, so verification of the sample position has to be done through image registration. The medium resolution CT scan showed big regional differences in porosity and dense mineral content (Figure 6), which means that it is important to know the location of the small subsample inside the big dataset. The scans at different resolutions reveal that multi-scale imaging is necessary to avoid inaccurate conclusions. Results illustrated that when the resolution gap between parent sample and sub-sample is too large, finding the location of the sub-sample in its parent is very hard to impossible, only based on the images. In this case additional information coming from SEM or other complementary techniques is a major aid, maybe even a necessity to make this 3D-to-3D image registration work.

After localization of the subsample, porosity of that area in the parent sample could be analyzed and was found to be 11.3 %, of which about 2 % was closed porosity. Compared to the 9 % porosity of the overall sample, it is clear that the subsample was

taken in a region with more than average porosity. However, 16 % can be interpreted as the correct porosity value, as the analysis error on the low-resolution data is just to high.

5. Conclusions

At present, no image-based analysis technique can be considered as a multi-scale, all-area characterization technique for heterogeneous porous media. A combination of different imaging techniques, both 2D and 3D, followed by intensive post-processing of the acquired images can be used to provide more complete information on the analyzed material.

In the proposed methodology, medium-resolution μ-CT results in three-dimensional, structural information of a large, centimeter-scale sample. Although the resolution is limited, large features can be identified, and interesting areas for further research are easily pinpointed. Data fusion of this medium-resolution 3D information with 2D imaging techniques such as SEM provide additional information in terms of structure. More importantly, the implementation of chemical analysis by means of EDS provides a pseudo-3D distribution of the different mineral phases present in the sample. Furthermore, SEM and EDS are mature and low-cost methods, accessible for most researchers in the field of materials characterization. Sub-sampling the material allows for imaging at higher resolutions using lab-based CT, but the limit of this technique still lays at a spatial resolution of about 0.5 μm. Since this is not enough to resolve the finest features inside the Vosges stone, other methods should be addressed. Future research will include data analysis on the Vosges sandstone from FIB-nt, high resolution synchrotron X-ray μ-CT and ptychographic tomography, focusing on the submicron porosity. FIB-nt, using secondary electron imaging, can achieve a spatial resolution of below 10 nm. High resolution μ-CT at synchrotron facilities can provide images with

resolutions below 100 nm (Kastner et al., 2010) and with ptychographic tomography (Dierolf et al., 2010), resolutions of up to 16 nm in 3D have been reached (Holler et al., 2014). In combination with the study presented in this paper, this will provide a complete workflow for the analysis of the multiscale pore space of sandstones. In all cases, coupling between different methods is a necessity, since the heterogeneity of natural materials causes the need for the exact localization of sub-samples in their parent sample. Image registration techniques in two or three dimensions have therefore become very important in image processing.

6. Acknowledgements

The Special Research Fund of Ghent University is acknowledged for the Ph.D. scholarship of Wesley De Boever.

Hannelore Derluyn is a postdoctoral fellow of the Research Foundation - Flanders (FWO) and acknowledges its support.

7. References

Al-Raoush, R., Papadopoulos, A., 2010. Representative elementary volume analysis of porous media using X-ray computed tomography. Powder Technol. 200, 69–77. doi:10.1016/j.powtec.2010.02.011

Antrett, P., 2013. Characterization of an Upper Permian Tight Gas Reservoir. Springer Theses 87–98. doi:10.1007/978-3-642-36294-1

Bésuelle, P., Desrues, J., Raynaud, S., 2000. Experimental characterisation of the localisation phenomenon inside a Vosges sandstone in a triaxial cell. Int. J. Rock Mech. Min. Sci. 37, 1223–1237. doi:10.1016/S1365-1609(00)00057-5

Bookstein, F.L., 1989. Size and shape spaces for landmark data in two dimensions. Stat. Sci. 1, 181–242.

Boone, M., Dewanckele, J., Cnudde, V., Silversmit, G., Van Ranst, E., Jacobs, P., Vincze, L., Van Hoorebeke, L., 2011. Three-dimensional phase separation and identification in granite. Geosphere 7, 79–86. doi:10.1130/ges00562.1

Brabant, L., Vlassenbroeck, J., De Witte, Y., Cnudde, V., Boone, M.N., Dewanckele, J., Van Hoorebeke, L., 2011. Three-Dimensional Analysis of High-Resolution X-Ray Computed Tomography Data with Morpho+. Microsc. Microanal. 17, 252–263. doi:10.1017/s1431927610094389

Cirpka, O., Leven, C., Schwede, R., Doro, K., Bastian, P., Ippisch, O., Klein, O., Patzelt, A., 2014. Tomographic Methods in Hydrogeology, in: Weber, M., Münch, U. (Eds.), Tomography of the Earth's Crust: From Geophysical Sounding to Real-Time Monitoring SE - 9, Advanced Technologies in Earth Sciences. Springer International Publishing, pp. 157–176. doi:10.1007/978-3-319-04205-3_9

Cnudde, V., Boone, M.N., 2013. High-resolution X-ray computed tomography in geosciences: A review of the current technology and applications. Earth-Science Rev. 123, 1–17. doi:10.1016/j.earscirev.2013.04.003

De Kock, T., Boone, M., Dewanckele, J., Boever, W. De, Boone, M., Schutter, G. De, Lehmann, E., 2013. Monitoring frost susceptibility of limestone faces, in: 12th International Congress on the Deterioration and Conservation of Stone.

Derluyn, H., Griffa, M., Mannes, D., Jerjen, I., Dewanckele, J., Vontobel, P., Sheppard, a., Derome, D., Cnudde, V., Lehmann, E., Carmeliet, J., 2013. Characterizing saline uptake and salt distributions in porous limestone with neutron radiography and X-ray micro-tomography. J. Build. Phys. 36, 353–374. doi:10.1177/1744259112473947

Dewanckele, J., De Kock, T., Boone, M.A., Cnudde, V., Brabant, L., Boone, M.N., Fronteau, G., Van Hoorebeke, L., Jacobs, P., 2012. 4D imaging and quantification of pore structure modifications inside natural building stones by means of high resolution X-ray CT. Sci. Total Environ. 416, 436–448. doi:10.1016/j.scitotenv.2011.11.018

Dewanckele, J., De Kock, T., Fronteau, G., Derluyn, H., Vontobel, P., Dierick, M., Van Hoorebeke, L., Jacobs, P., Cnudde, V., 2014. Neutron radiography and X-ray computed tomography for quantifying weathering and water uptake processes inside porous limestone used as building material. Mater. Charact. 88, 86–99. doi:10.1016/j.matchar.2013.12.007

Dierolf, M., Menzel, A., Thibault, P., Schneider, P., Kewish, C.M., Wepf, R., Bunk, O., Pfeiffer, F., 2010. Ptychographic X-ray computed tomography at the nanoscale. Nature 467, 436–9. doi:10.1038/nature09419

Gall, J.-C., Grauvogel-Stamm, L., 2005. The early Middle Triassic “Grès à Voltzia” Formation of eastern France: a model of environmental refugium. Comptes Rendus Palevol 4, 637–652. doi:10.1016/j.crpv.2005.04.007

Holler, M., Diaz, a, Guizar-Sicairos, M., Karvinen, P., Färm, E., Härkönen, E., Ritala, M., Menzel, a, Raabe, J., Bunk, O., 2014. X-ray ptychographic computed tomography at 16 nm isotropic 3D resolution. Sci. Rep. 4, 3857. doi:10.1038/srep03857

Holzer, L., Indutnyi, F., Gasser, P.H., Münch, B., Wegmann, M., 2004. Three-dimensional analysis of porous BaTiO3 ceramics using FIB nanotomography. J. Microsc. 216, 84–95. doi:10.1111/j.0022-2720.2004.01397.x

Huddlestone-Holmes, C.R., Ketcham, R. a., 2005. Getting the inside story: Using computed X-ray tomography to study inclusion trails in garnet porphyroblasts. Am. Mineral. 90, 1918. doi:10.2138/am.2005.1840

Jiao, K., Yao, S., Liu, C., Gao, Y., Wu, H., Li, M., Tang, Z., 2014. The characterization and quantitative analysis of nanopores in unconventional gas reservoirs utilizing FESEM–FIB and image processing: An example from the lower Silurian Longmaxi Shale, upper Yangtze region, China. Int. J. Coal Geol. 128-129, 1–11. doi:10.1016/j.coal.2014.03.004

Jussiani, E.I., Appoloni, C.R., 2014. Effective atomic number and density determination of rocks by X-ray microtomography. Micron 70C, 1–6. doi:10.1016/j.micron.2014.11.005

Kastner, J., Harrer, B., Requena, G., Brunke, O., 2010. A comparative study of high resolution cone beam X-ray tomography and synchrotron tomography applied to Fe- and Al-alloys. NDT E Int. 43, 599–605. doi:10.1016/j.ndteint.2010.06.004

Keller, L.M., Holzer, L., Wepf, R., Gasser, P., Münch, B., Marschall, P., 2011. On the application of focused ion beam nanotomography in characterizing the 3D pore space geometry of Opalinus clay. Phys. Chem. Earth, Parts A/B/C 36, 1539–1544. doi:10.1016/j.pce.2011.07.010

Ketcham, R.A., Carlson, W.D., 2001. Acquisition, optimization and interpretation of X-ray computed tomographic imagery: applications to the geosciences. Comput. Geosci. 27, 381–400.

Lagrou, D., Dreesen, R., Broothaers, L., 2004. Comparative quantitative petrographical analysis of Cenozoic aquifer sands in Flanders (N Belgium): overall trends and quality assessment. Mater. Charact. 53, 317–326. doi:10.1016/j.matchar.2004.07.012

Masschaele, B., Dierick, M., Loo, D. Van, Boone, M.N., Brabant, L., Pauwels, E., Cnudde, V., Hoorebeke, L. Van, 2013a. HECTOR: A 240kV micro-CT setup optimized for research. J. Phys. Conf. Ser. 463, 012012. doi:10.1088/1742-6596/463/1/012012

Masschaele, B., Dierick, M., Loo, D. Van, Boone, M.N., Brabant, L., Pauwels, E., Cnudde, V., Hoorebeke, L. Van, 2013b. HECTOR: A 240kV micro-CT setup optimized for research. J. Phys. Conf. Ser. 463, 012012. doi:10.1088/1742-6596/463/1/012012

Matsuoka, N., Murton, J., 2008. Frost weathering: Recent advances and future directions. Permafr. Periglac. Process. 19, 195–210. doi:10.1002/ppp.620

Nijland, T.G., Dubelaar, C.W., Wijffels, T.J., van der Linden, T.J.M., 2004. Zwartverkleuring van Bentheimer, Obernkirchener en Rakowicze zandsteen. Prakt. Instandhouding Monum. Deel II-4 .

Reed, S.J.B. (University of C., 2005. Electron Microprobe Analysis and Scanning Electron Microscopy in Geology.

Schmitt, L., Forsans, T., Santarelli, F.J., 1994. Shale Testing and Capillary Phenomena. Int. J. Rock Mech. Min. Sci. 31, 411–427.

Shear, W. a., Selden, P. a., Gall, J.-C., 2009. Millipedes from the Grès à Voltzia, Triassic of France, with comments on Mesozoic millipedes (Diplopoda: Helminthomorpha: Eugnatha). Int. J. Myriap. 2, 1–13. doi:10.1163/187525409X462395

Sok, R.M., Varslot, T., Ghous, A., Latham, S., Sheppard, A.P., Knackstedt, M.A., 2010. Pore Scale Characterization of Carbonates at Multiple Scales: Integration of Micro-CT, BSEM, and FIBSEM. Petrophysics 51, 379–387.

Vlassenbroeck, J., Dierick, M., Masschaele, B., Cnudde, V., Hoorebeke, L., Jacobs, P., 2007. Software tools for quantification of X-ray microtomography. Nucl. Instruments Methods Phys. Res. Sect. a-Accelerators Spectrometers Detect. Assoc. Equip. 580, 442–445. doi:10.1016/j.nima.2007.05.073

Wildenschild, D., Sheppard, A.P., 2013. X-ray imaging and analysis techniques for quantifying pore-scale structure and processes in subsurface porous medium systems. Adv. Water Resour. 51, 217–246. doi:http://dx.doi.org/10.1016/j.advwatres.2012.07.018

1